Lecture Notes in Physics

8

Proceedings of the Second International Conference on Numerical Methods in Fluid Dynamics

September 15–19, 1970
University of California, Berkeley
Edited by Maurice Holt

Springer-Verlag
Berlin · Heidelberg · New York 1971

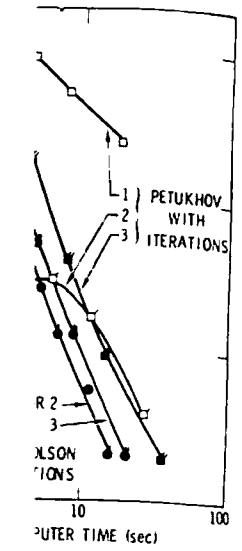

TIONS ON THE ABSOLUTE ERROR
ASS FRACTION OF ATOMS AT
FLAT PLATE

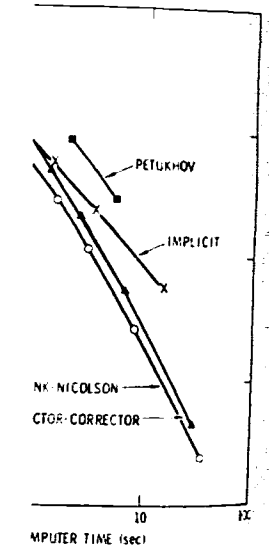

E ERROR IN STANTON NUMBER
= 3 FOR HYPERBOLOID

NUMERICAL SOLUTION OF THE INTERACTION OF A SHOCK WAVE WITH A LAMINAR BOUNDARY LAYER

Robert W. MacCormack
Ames Research Center, NASA
Moffett Field, Calif. 94035

INTRODUCTION

Currently many problems of fluid dynamics are being attacked by finite difference techniques. In the numerical solution of any given problem, several questions are raised concerning the accuracy or quality of the computed solution. Unfortunately too few of these questions have answers. Accuracy depends on the order of accuracy of the numerical method (consistency), numerical stability, matching of both the numerical and physical domains of dependence (to be discussed herein), and on simulating numerically all of the physically significant processes in the flow field. In addition to accuracy, the numerical analyst is also concerned with obtaining the solution as efficiently as possible. The purpose of this paper is to examine the numerical behavior of an efficient Lax-Wendroff difference technique of second order accuracy now being used to solve a wide range of problems in fluid dynamics (MacCormack, 1969; Kutler, 1969). In particular, this technique will be modified to meet the specific demands required for the solution of the interaction of a shock wave with a laminar boundary layer. The modified techniques, obtained through the concept of splitting, may however themselves have a much wider application in the solution of problems in fluid dynamics.

GENERAL NUMERICAL CONSIDERATIONS

The time-dependent Navier-Stokes equations, in two dimensions, neglecting body forces and heat sources, may be written in vector form as

$$\frac{\partial U}{\partial t} + \frac{\partial F}{\partial x} + \frac{\partial G}{\partial y} = 0 \tag{1}$$

where $U = \begin{pmatrix} \rho \\ \rho u \\ \rho v \\ e \end{pmatrix}$, $F = \begin{pmatrix} \rho u \\ \rho u^2 + \sigma_x \\ \rho uv + \tau_{xy} \\ (e + \sigma_x)u + \tau_{yx}v + k\frac{\partial T}{\partial x} \end{pmatrix}$, $G = \begin{pmatrix} \rho v \\ \rho uv + \tau_{yx} \\ \rho v^2 + \sigma_y \\ (e + \sigma_y)v + \tau_{xy}u + k\frac{\partial T}{\partial y} \end{pmatrix}$

$$\sigma_x = p - \lambda\left(\frac{\partial u}{\partial x} + \frac{\partial v}{\partial y}\right) - 2\mu\frac{\partial u}{\partial x}, \quad \tau_{xy} = \tau_{yx} = -\mu\left(\frac{\partial u}{\partial y} + \frac{\partial v}{\partial x}\right) \text{ and } \sigma_y = p - \lambda\left(\frac{\partial u}{\partial x} + \frac{\partial v}{\partial y}\right) - 2\mu\frac{\partial v}{\partial y}$$

for density ρ, x and y velocity components u and v, viscosity coefficients λ and μ, total energy per unit volume e, specific internal energy ϵ, coefficient of heat conductivity k, and temperature T. Finally, the pressure p is related to ϵ and ρ by an equation of state, $p(\epsilon,\rho)$, where $\epsilon = e/\rho - (u^2 + v^2)/2$.

A two-step difference method of second order accuracy (MacCormack, 1969) devised to solve Eq. (1) can be defined by

$$\left.\begin{aligned} \overline{U^{n+1}_{i,j}} &= U^n_{i,j} - \frac{\Delta t}{\Delta x}\left(F^n_{i+1,j} - F^n_{i,j}\right) - \frac{\Delta t}{\Delta y}\left(G^n_{i,j+1} - G^n_{i,j}\right) \\ U^{n+1}_{i,j} &= \frac{1}{2}\left\{U^n_{i,j} + \overline{U^{n+1}_{i,j}} - \frac{\Delta t}{\Delta x}\left(\overline{F^{n+1}_{i,j}} - \overline{F^{n+1}_{i-1,j}}\right) - \frac{\Delta t}{\Delta y}\left(\overline{G^{n+1}_{i,j}} - \overline{G^{n+1}_{i,j-1}}\right)\right\} \end{aligned}\right\} \tag{2}$$

where $F^n_{i,j}$ and $G^n_{i,j}$ equal $F(U^n_{i,j})$ and $G(U^n_{i,j})$. The subscripts refer to a spacial mesh of points (x_i,y_j) with spacing Δx and Δy, and the superscripts refer to times $t = n\Delta t$ where Δt is the time increment that the solution is advanced during each cycle of Eqs. (2). The method first obtains an approximate value, $\overline{U^{n+1}_{i,j}}$, at each point using two forward differences to approximate the two spacial derivatives. The approximate solution is then used in the second equation, using two backward differences, to obtain the new accepted value $U^{n+1}_{i,j}$. The above difference method is only one of four methods of essentially the same form. For example, if instead of first using two forward spacial differences and then two backward differences, the reverse procedure could be followed or one forward and one backward difference could be followed by corresponding backward and forward differences. The

variant defined by Eqs. (2) will be used here only to illustrate the numerical behavior common to all four and it should be used to solve Eq. (1) with caution, as will become clear later in the section on accuracy and stability.

For the analysis of the numerical behavior, in particular, stability, of the difference equations, only the inviscid non-heat-conducting equations will be treated in detail. Both the viscous and heat conduction terms, physically and also numerically (if their magnitudes in the differenced equations are not too great), tend to damp out the high frequency components of the solution, which are normally the ones which cause numerical instability. Thus, it is expected that the inclusion of these terms in the analysis would only enhance stability.

Domain of Numerical Dependence

To advance the solution in time by Δt at one mesh point (x_j, y_j), using Eqs. (2), requires knowledge of only seven neighboring points. This "star" of points is illustrated in Fig. 1. The points marked A are primary in that information at these points more strongly modifies the solution at (x_j, y_j) during time Δt than does that at points B. The three other variants of Eqs. (2) have similar stars; the only differences are in the locations of the points B. The seven points define the numerical domain of dependence. The first requirement of any method is that its numerical domain include the physical domain of dependence. Clearly, if this is violated, the numerical scheme does not have in hand all the data necessary to advance the solution in time. On the other hand, there are two reasons why the numerical domain should not be much larger than the physical domain. First, to obtain an accurate numerical solution at a given point which "sees" much more data with time than the true solution, a rather severe demand is made of the numerical method to ignore or give little weight to the extraneous data. Second, the computation time spent in processing this unneeded data is costly. If the more restrictive domain, the primary domain defined by the points A (cross-hatched in Fig. 1) is taken as the effective numerical domain, the above requirement is met if

$$\Delta t \le (|u|/\Delta x + |v|/\Delta y + c\sqrt{1/\Delta x^2 + 1/\Delta y^2})^{-1} \tag{3}$$

where c is the local adiabatic speed of sound. This condition is usually called the Courant-Friedrich-Lewy (C.F.L.) condition.

Accuracy and Stability

The numerical stability of methods of this type, namely, those of the Lax-Wendroff class, cannot presently be completely analyzed in the general nonlinear form. The most successful attempt to date is to first linearize the set of differential Eqs. (1) and then to study the amplification of Fourier components of the solution by the difference method applied to the linearized set. The new set is then

$$\frac{\partial U}{\partial t} + J_F \frac{\partial U}{\partial x} + J_G \frac{\partial U}{\partial y} = 0 \tag{4}$$

where J_F and J_G are the Jacobian matrices of F and G with respect to U and are considered to be constant. This set of equations approximates Eqs. (1) locally, and difference methods found to be unstable for it can be expected to be unstable for the general nonlinear case. Two conditions inherent in such an analysis are: (a) the boundary conditions have no effect on stability, and (b) the exact solution to Eq. (1) is smooth. The latter condition allows the matrices J_F and J_G to be treated as constants (locally).

The amplification matrix of the difference Eqs. (2) applied to Eqs. (4) for a single Fourier component of the solution, $W(t)\exp[i(k_1x+k_2y)]$, becomes

$$\mathcal{G} = I - i\Delta t\left(\frac{J_F}{\Delta x}\sin\xi + \frac{J_G}{\Delta y}\sin\eta\right) - \frac{1}{2}\Delta t^2\left(\frac{J_F}{\Delta x}(1 - e^{-i\xi}) + \frac{J_G}{\Delta y}(1 - e^{-i\eta})\right)\left(\frac{J_F}{\Delta x}(1 - e^{i\xi}) + \frac{J_G}{\Delta y}(1 - e^{i\eta})\right)$$

where $\xi = k_1\Delta x$ and $\eta = k_2\Delta y$. For ξ and $\eta \ll 1$, $\mathcal{G} = \exp[-i\Delta t(J_F\xi/\Delta x + J_G\eta/\Delta y)]$ modulo terms of third order in ξ and η. The exact solution of Eqs. (4) for the above Fourier component is $\exp[-it(k_1J_F + k_2J_G)]\exp[i(k_1x + k_2y)]W(0)$. Hence, the exact amplification of the solution from $t = 0$ to $t = \Delta t$ is $\exp[-it(k_1J_F + k_2J_G)]$ which equals $\mathcal{G}$ modulo terms of third order in ξ and η. Thus the difference method is shown to be of second order accuracy.

In the limiting process $\Delta t \to 0$, stability is assured if all the eigenvalues, λ_i, of $\mathcal{G}$ satisfy the von Neumann condition

$$|\lambda_i| \leq 1 + O(\Delta t) \tag{5}$$

The eigenvalues of $\mathcal{G}$ are invariant under a similarity transformation. There exists a transformation, S, such that $\mathcal{G}' = S^{-1}\mathcal{G}S = I + K - K^* - 2K^*K$,[1] where

$$K = (\Delta t/2)\left((1 - e^{i\xi})A/\Delta x + (1 - e^{i\eta})B/\Delta y\right)$$

$$A = \begin{pmatrix} u & c & 0 & 0 \\ c & u & 0 & 0 \\ 0 & 0 & u & 0 \\ 0 & 0 & 0 & u \end{pmatrix} \text{ and } B = \begin{pmatrix} v & 0 & c & 0 \\ 0 & v & 0 & 0 \\ c & 0 & v & 0 \\ 0 & 0 & 0 & v \end{pmatrix}$$

It can be shown that $|(w,\mathcal{G}'w)|^2 \leq 1 + 4||Kw||^4$ where w is any unit vector, $(w,\mathcal{G}'w)$ is the inner product of w with $\mathcal{G}'w$ and $||Kw|| = (Kw,Kw)^{1/2}$; hence the eigenvalues of $\mathcal{G}$ can be made to satisfy (5) as $\Delta t \to 0$ if $\Delta t^3/\Delta x^4$ is held fixed. It can be shown that the bound on $|(w,\mathcal{G}'w)|^2$ is a least upper bound (i.e., the value is achieved by $(w,\mathcal{G}'w)$) by considering $v = -(\Delta y/\Delta x)u$, $\xi = -\eta$ and $w = (1,0,0,0)^T$. Then $|(w,\mathcal{G}'w)|^2 = 1 + 4(\sin \xi \Delta t u/\Delta x)^4$. The fixing of $\Delta t^3/\Delta x^4$ as $\Delta t \to 0$ is much more restrictive than the condition imposed by the C.F.L. condition (Eq. (3)). It is a necessary condition near the unfavorable velocity directions $v = -u\Delta y/\Delta x$. The other three variants also have unfavorable directions: however they are not all the same. The amplification matrix of each has in general different eigenvalues and vectors for each Fourier component of the solution; hence a single component would not in general maximize $|(w,\mathcal{G}w)|$ for each variant.

It was conjectured that if the four variants followed one another cyclically during the numerical calculation, the condition on Δt would be close to that of the C.F.L. condition. The difference method is then in terms of the permutted subscripts ii and jj and the mod function[2]

$$\left.\begin{aligned} ii &= \text{mod}\,(n,2) \\ jj &= \text{mod}\,(n - ii,4)/2 \\ U_{i,j}^{\overline{n+1}} &= U_{i,j}^{n} - \frac{\Delta t}{\Delta x}\left(F_{ii,j}^{n} - F_{ii-1,j}^{n}\right) - \frac{\Delta t}{\Delta y}\left(G_{i,jj}^{n} - G_{i,jj-1}^{n}\right) \\ ii &= \text{mod}\,(ii + 1,2) \\ jj &= \text{mod}\,(jj + 1,2) \\ U_{i,j}^{n+1} &= \frac{1}{2}\left\{U_{i,j}^{n} + U_{i,j}^{\overline{n+1}} - \frac{\Delta t}{\Delta x}\left(F_{ii,j}^{\overline{n+1}} - F_{ii-1,j}^{\overline{n+1}}\right) - \frac{\Delta t}{\Delta y}\left(G_{i,jj}^{\overline{n+1}} - G_{i,jj-1}^{\overline{n+1}}\right)\right\} \end{aligned}\right\} \tag{6}$$

It has not yet been possible to assess the validity of the conjecture analytically. Instead the eigenvalue least upper bound for several flow directions will be approximated using a power method and a simple numerical test problem. Consider a region of uniform flow containing a square array of mesh points, $U_{i,j}^{o}$ = constant, i, j = 1,2, . . . , N. Using the similarity transformation S on Eq. (4), we have

$$\frac{\partial Z}{\partial t} + A\frac{\partial Z}{\partial x} + B\frac{\partial Z}{\partial y} = 0 \tag{7}$$

where $Z = S^{-1}U$. The exact solution is $Z(t) = S^{-1}U(t) = S^{-1}U^o = Z^o$. Let L denote the numerical operator which obtains U^{n+1} from U^n according to Eqs. (6) and also where the inflow boundary point values are fixed and the outflow boundary point values are calculated using backward or, more precisely, upstream differencing. In the absence of roundoff error, since the technique defined by Eqs. (6) is consistent (of second order), $Z^{n+1} = LZ^n = (L)^nZ^o = Z^o$. The numerical solution is exact. Now let δ^o be a perturbation to Z^o rich in Fourier components which can be supported by the mesh. With $Z^o + \delta^o$ as an initial condition, by

[1]The superscripts * and T denote complex conjugate and transpose.

[2]The function mod (x,y) is defined as x - [x/y]y where [x/y] is the integral part of x/y.

linearity, both the set of differential Eqs. (7) and the difference equations reduce to

$$\frac{\partial \delta}{\partial t} + A\frac{\partial \delta}{\partial x} + B\frac{\partial \delta}{\partial y} = 0 \qquad \text{and} \qquad \delta^{n+1} = L\delta^{n} = (L)^{n}\delta^{o}$$

As earlier in this section, the magnitude of the exact amplification of each component of δ is unity. On the other hand, if all the eigenvalues of the amplification matrix $\mathcal{G}_L$ associated with the operator L are less than or equal to one in magnitude $||\delta^{n+1}|| \leq ||\delta^{o}||$; otherwise $||\delta^{n+1}||$ will grow exponentially with n. The numerical results for Mach number 2.0, a mesh of 20 x 20 points, $\delta^{o}_{i,j} = (0,0,0,0)^{T}$ for $i \neq 10$ and $j \neq 10$ and $\delta^{o}_{10,10} = (0,1,0,1)^{T}$ are contained in Fig. 2 for $\Delta y/\Delta x = 1$ and for $\Delta y/\Delta x = 0.1$ (the form of $\delta^{o}_{10,10}$ is explained in footnote 3). Each point of the figures represents the result of a numerical solution, δ^{n}, and is plotted in polar coordinates with $c\Delta t/\Delta x$ as the radial coordinate and arctan v/u as the angular coordinate. Each solution was advanced from 40 to 400 time steps until it could be determined if $||\delta^{n}||$ remained bounded by unity (open symbols) or grew exponentially (closed symbols). The closed curve of each figure represents the C.F.L. condition, Eq. (3), with the equality sign. These results indicate that the C.F.L. condition is a sufficient condition for the stability of the difference Eqs. (6). Also, Fig. 2(a) shows that for the difference Eqs. (2), the associated amplification matrix has eigenvalues greater than one in magnitude for the velocity directions $3\pi/4$ and $7\pi/4$. However, it was observed that at arctan $v/u = 0$, $\pi/4$, $\pi/2$, π, $5\pi/4$ and $3\pi/2$ the associated eigenvalues of Eqs. (2) were bounded by unity if $c\Delta t/\Delta x$ satisfied the C.F.L. condition.

A Nonlinear Instability

Difference schemes shown to be stable by linear analysis may still experience numerical difficulties in the solution of nonlinear problems. Normally they appear where linear theory does not apply, in particular in regions where the exact solution is not smooth. However, even in smooth regions difficulties can occur. To demonstrate this, consider the equation $\frac{\partial \rho u}{\partial t} + \frac{\partial \rho u^2}{\partial x} = 0$, where ρ is constant, and the finite difference approximation to it,

$$u_i^{n+1} = u_i^{n} - (\Delta t/\Delta x)\left\{\left(\rho u^2\right)^{n}_{i+1/2} - \left(\rho u^2\right)^{n}_{i-1/2}\right\}$$

where $\left(\rho u^2\right)^{n}_{i+1/2}$ may be ρu^{n2}_{i+1} (forward difference), or ρu_i^{n2} (backward difference) or $\left(\rho u_i^{n2} + \rho u^{n2}_{i+1}\right)/2$ (central difference). Viewing the mesh as composed of cells allows the following interpretation of the difference equation. The change in ρu_i during time Δt is equal to the difference in momentum transported across the cell face located at $x = (i + 1/2)\Delta x$ from that at $x = (i - 1/2)\Delta x$. Let us consider only the effect of transport across the cell face at $x = (i + 1/2)\Delta x$ and suppose that both u_i^{n} and u^{n}_{i+1} are nonzero. There are four cases to consider: (a) $u_i^{n}, u^{n}_{i+1} < 0$; (b) $u_i^{n}, u^{n}_{i+1} > 0$; (c) $u_i^{n} > 0$, $u^{n}_{i+1} < 0$; and (d) $u_i^{n} < 0$, $u^{n}_{i+1} > 0$.

For case (a), cell i containing negative momentum receives $-(\Delta t/\Delta x)(\rho u^2)^{n}_{i+1/2}$ momentum per unit volume from cell i + 1, the "donor cell." The magnitude of momentum of the receiving cell is increased while that of the donor cell is decreased. Thus the difference equation is consistent with the physics of the flow at the cell face. The reduction in magnitude of the donor cell is a stabilizing influence. Case (b) is essentially the same as case (a) with the roles of cells i and i + 1 reversed. In case (c) both cells are donors and because $\rho u_i^{n} > 0$ and $\rho u^{n}_{i+1} < 0$, the magnitudes of momentum of both cells are reduced, again a stabilizing process. Case (d) exhibits an entirely different behavior. Both cells are receivers, increase their momentum magnitude by $(\Delta t/\Delta x)(\rho u^2)^{n}_{i+1/2}$ during time Δt and will again satisfy the requirements for case (d) for the next time step. Thus, this process is self-aggravating, a destabilizing influence. The difficulty arises because the difference equation loses information about the sign of u^{n}_{i+1} through squaring. For cell i the difference equation cannot distinguish case (d) from case (a) or for cell i + 1 case (d) from case (b). Thus the difference

[3] The fourth equation of Eqs. (7) is not coupled to the first three; hence it needs to be directly perturbed. The first three are coupled; hence a perturbation to any one will perturb the other two.

equation can violate the physics of the flow by allowing a quantity of negative momentum to be transported out of a cell, possibly containing only positive momentum, through a surface at which u vanishes. This numerical difficulty, when encountered can be remedied by appealing to the physics of the flow. The fluid velocity at the cell face can be approximated to second order accuracy by $(u_i^n + u_{i+1}^n)/2$ and if the term $(\rho u^2)_{i+1/2}^n$ is replaced in the difference equation by $\{(u_i^n + u_{i+1}^n)/2\}(\rho u)_{i+1/2}^n$ where $(\rho u)_{i+1/2}^n$ is defined as before, the order of accuracy of the difference equation is unchanged. The modification reduces the destabilizing influence because $\{(u_i^n + u_{i+1}^n)/2\}(\rho u)_{i+1/2}^n < (\rho u^2)_{i+1/2}^n$ and also is more consistent with the physics of the flow. This modification is employed when the conditions of case (d) occur by the methods described in this paper.

SPECIFIC NUMERICAL CONSIDERATIONS

In this section the ideas and techniques of the previous section will be tailored to meet the specific needs for the solution of the interaction of a shock wave with a laminar boundary layer on a flat plate sketched in Fig. 3. In the process some ideas are developed which may be very significant in the numerical solution of fluid dynamic problems in general.

As in any problem, the primary necessity is to choose Δx and Δy small enough so that: (1) good spatial resolution of the features in the flow field is attained; and (2) all the significant physical processes, for example, viscous shear, are exhibited without being largely influenced by truncation error. Unfortunately, it is impossible without knowing the exact solution and its derivatives to choose Δx and Δy so that these requirements are sure to be achieved.

This particular flow problem has characteristic lengths normal to the plate (y-direction), boundary layer thickness, and along the plate (x-direction), the distance from the leading edge to the incident shock, x_s, differing by several orders of magnitude. One approach to meet the above needs is to choose Δx and Δy so that all of the significant terms of the set of differential equations are all of nearly the same magnitude in the set of difference equations. For example, consider the transport term $(\partial \rho vu/\partial y)$ and the viscous stress term $\frac{\partial \mu \frac{\partial u}{\partial y}}{\partial y}$ of the x-direction momentum equation.[4] If we linearize and difference them, we have[5] $\frac{\rho v}{2\Delta y}(u_{j+1} - u_{j-1})$ and $(\mu/\Delta y^2)(u_{j+1} - 2u_j + u_{j-1})$. Equating the coefficients of these difference terms results in $\rho v \Delta y/\mu = 2$, a mesh Reynolds number, $Re_{\Delta y}$, of two. Comparing this number with the free-stream Reynolds number, Re_{x_s}, we obtain the estimate

$$\Delta y \approx \frac{Re_{\Delta y}}{Re_{x_s}} \frac{u_o}{v} x_s \approx \frac{2u_o x_s}{v Re_{x_s}} \tag{8}$$

where u_o is the free-stream velocity and it is assumed that the kinematic viscosity, μ/ρ, varies little from that of the free stream. Now estimating Δx, we, as before, linearize and difference the terms $\frac{\partial \rho u^2}{\partial x}$ and $\frac{\partial \rho vu}{\partial y}$. Equating the coefficients of the difference terms yields

$$\Delta x = \frac{u}{v} \Delta y \tag{9}$$

In using Eqs. (8) and (9) to calculate mesh spacing in a region in which viscous phenomena are important, velocities u and v characteristic of the region will also have to be estimated. It is probable that the "equal in magnitude" of the difference coefficients could be relaxed to "of the same order of magnitude" without the viscous terms being swamped by truncation

[4]The choice of the x-direction momentum equation is consistent with the usual boundary layer analysis. The y-direction momentum equation normally reduces in the boundary layer equations to $\frac{\partial p}{\partial y} = 0$.

[5]A central difference approximation is used here because the use of one forward and one backward difference by the techniques of this paper during each time step is effectively that of using a central difference.

error. For this reason and the assumption about kinematic viscosity Eqs. (8) and (9) are believed to be conservative. Nevertheless, in the boundary layer region Δy is expected to be much smaller than Δx.

At moderate Mach numbers, if $\Delta y \ll \Delta x$, the calculation for Δt using the C.F.L. Eq. (3) is dominated by small y-direction mesh spacing. If Eqs. (6) are used to advance the solution, during each Δt, the numerical domain increases in the x and y directions by Δx and Δy. The physical domain increases in the y-direction by $(|v| + c)\Delta t \approx \Delta y$. However, in the x-direction, the increase is only $(|u| + c)\Delta t \ll \Delta x$. Thus the numerical domain is much larger than the physical domain. However, it is possible to modify Eqs. (6) using the concept of splitting so that this difficulty is avoided.

Splitting

The concept of splitting is originally due to Peaceman and Rachford (1955) and is commonly known as the method of alternating directions. Since then, it has been widely used (Yanenko, 1969) to transform complex operators into a sequence of simpler ones. This concept will now be used to reduce the set of two dimensional Eqs. (6) into two sets of one-dimensional equations while maintaining second order accuracy.

Eqs. (6) can be split as follows:

$$
\left.
\begin{aligned}
&ii = \text{mod}\,(n,2)\\
&jj = \text{mod}\,(n - ii,4)/2\\
&\overline{U_{i,j}^{n+1/2}} = U_{i,j}^{n} - \left(\frac{\Delta t}{\Delta y}\right)\left(G_{i,jj}^{n} - G_{i,jj-1}^{n}\right)\\
&jj = \text{mod}\,(jj + 1,2)\\
&U_{i,j}^{n+1/2} = \frac{1}{2}\left\{U_{i,j}^{n} + \overline{U_{i,j}^{n+1/2}} - \frac{\Delta t}{\Delta y}\left(\overline{G_{i,jj}^{n+1/2}} - \overline{G_{i,jj-1}^{n+1/2}}\right)\right\}\\
&\overline{U_{i,j}^{n+1}} = U_{i,j}^{n+1/2} - \frac{\Delta t}{\Delta x}\left(F_{ii,j}^{n+1/2} - F_{ii-1,j}^{n+1/2}\right)\\
&ii = \text{mod}\,(ii + 1,2)\\
&U_{i,j}^{n+1} = \frac{1}{2}\left\{U_{i,j}^{n+1/2} + \overline{U_{i,j}^{n+1}} - \frac{\Delta t}{\Delta x}\left(\overline{F_{ii,j}^{n+1}} - \overline{F_{ii-1,j}^{n+1}}\right)\right\}
\end{aligned}
\right\} \quad (10)
$$

Letting L_y denote the operator which obtains $U^{n+1/2}$ from U^n and L_x that which obtains U^{n+1} from $U^{n+1/2}$ we have schematically $U^{n+1} = L_x L_y U^n$. It can be shown that because of the noncommutativity of L_x and L_y that the numerical method $L_x L_y$ is only of first order. However, it will now be shown that the method defined by $U^{n+2} = L_y L_x L_x L_y U^n$ is of second order accuracy.

The amplification matrix associated with L_x is $\mathcal{G}_x = I - i(\Delta t J_F/\Delta x)\sin\xi - (\Delta t J_F/\Delta x)^2(1 - \cos\xi)$. The eigenvalues of J_F are the same as A, u, u, $u \pm c$ and those of $\mathcal{G}_x$ are less than or equal to unity in magnitude if $\Delta t \le \Delta t_x = \Delta x/(|u| + c)$. Similarly, $\mathcal{G}_y = I - i(\Delta t J_G/\Delta y)\sin\eta - (\Delta t J_G/\Delta y)^2(1 - \cos\eta)$ and its eigenvalues are less than or equal to one in magnitude if $\Delta t \le \Delta t_y = \Delta y/(|v| + c)$. Thus Eqs. (10) are stable if $\Delta t \le \min(\Delta t_y, \Delta t_x)$, since each component operator is then stable. Now for $\xi, \eta \ll 1$, $\mathcal{G}_y \mathcal{G}_x \mathcal{G}_x \mathcal{G}_y = \exp[-i2\Delta t(J_F\xi/\Delta x + J_G\eta/\Delta u)]$, the exact amplification of the solution during $2\Delta t$, modulo terms of third order in ξ and η. The extension to three dimensions, $L_z L_y L_x L_x L_y L_z$, is simple.

Now suppose that $\Delta y \ll \Delta x$ so that $\Delta t_y/\Delta t_x \ll 1$. Let $L_x(\Delta t_x)$ be L_x as before with $\Delta t = \Delta t_x$, $L_y(\Delta t_y)$ be similarly defined and M be the smallest even integer greater than $\Delta t_x/\Delta t_y$. Then the following method of second order accuracy advances the numerical solution Δt_x in time.

$$U^{n-1} = (L_y(\Delta t_x/M))^{M/2}\, L_x(\Delta t_x)\, (L_y(\Delta t_x/M))^{M/2}\, U^n$$

(In a chain of time steps this operator is $\ldots L_y^M L_x L_y^M L_x \ldots$.) The advantages of this split

technique are: (a) For M time step advances in the "y-direction" where Δt_y is at least as large as the maximum allowed by Eq. (3), the "x-direction" terms, $\frac{\partial F}{\partial x}$, need only be computed once, as compared with M times with Eqs. (6) and (b) the physical and numerical domains of dependence are matched more closely, since during time Δt_x both domains increase by $(|u| + c)\Delta t_x = \Delta x$ in the x-direction and in the y-direction the physical domain increases by $(|v| + c)\Delta t_x \approx (|v| + c)M\Delta t_y = M\Delta y$ which is the numerical domain increase. The main disadvantage for large M is that the solution is advanced in the y-direction many times nearly completely independent of the nature of the solution in the x-direction. Although this small amount of coupling becomes unimportant in the limit as $\Delta x, \Delta y \to 0$, at practical choices of Δx and Δy this need not be the case. This difficulty can be overcome while retaining the advantages of splitting as follows. First, the term $\frac{\partial F}{\partial x}$ will be calculated at time $(n + 1/2)\Delta t_x$ to second order accuracy by Eqs. (6) using $\Delta t = \Delta t_x$. $\left(\frac{\partial F}{\partial x}\right)^{n+1/2}_{i,j} = \frac{1}{2}\left(F^n_{ii,j} - F^n_{ii-1,j} + F^{\overline{n+1}}_{ii,j} - F^{\overline{n+1}}_{ii-1,j}\right)/\Delta x$. Let $L_{xy}(m, \Delta t)$ be the operator defined by

$$
\left.
\begin{aligned}
& jj = \mathrm{mod}\,(m, 2) \\
& U^{\overline{n+\frac{m+1}{M}}}_{i,j} = U^{n+\frac{m}{M}}_{i,j} - \frac{\Delta t}{\Delta y}\left(G^{n+\frac{m}{M}}_{i,jj} - G^{n+\frac{m}{M}}_{i,jj-1}\right) - \Delta t\left(\frac{\partial F}{\partial x}\right)^{n+1/2}_{i,j} \\
& jj = \mathrm{mod}\,(jj + 1, 2) \\
& U^{n+\frac{m+1}{M}}_{i,j} = \frac{1}{2}\left\{U^{n+\frac{m}{M}}_{i,j} + U^{\overline{n+\frac{m+1}{M}}}_{i,j} - \frac{\Delta t}{\Delta y}\left(G^{\overline{n+\frac{m+1}{M}}}_{i,jj} - G^{\overline{n+\frac{m+1}{M}}}_{i,jj-1}\right) - \Delta t\left(\frac{\partial F}{\partial x}\right)^{n+1/2}_{i,j}\right\} \\
& m = 0, 1, \ldots, M-1
\end{aligned}
\right\} \quad (11)
$$

Then the solution U^n is advanced in time by Δt_x by the following sequence:

(1) Calculate $\left(\frac{\partial F}{\partial x}\right)^{n+1/2}_{i,j}$ all i, j (2) $U^{n+1} = \prod_{m=0}^{M-1} L_{xy}(m, \Delta t_x/M)\, U^n$

where Π denotes the product. It is not difficult to show, using Taylor series expansions, that the above technique is of second order accuracy. For stability, if we again consider the linear case, $U^{n+\frac{m+1}{M}}_{i,j} = L_{xy}(m, \Delta t_x/M)\, U^{n+\frac{m}{M}}_{i,j} = L_y(\Delta t_x/M) + \frac{\Delta t_x}{M} C^{n+1/2}_{i,j}$, where $C^{n+1/2}_{i,j} = -\left(\frac{\partial F}{\partial x}\right)^{n+1/2}_{i,j} + \left(\Delta t_x J_G/(2M\Delta y)\right)\left\{\left(\frac{\partial F}{\partial x}\right)^{n+1/2}_{i,jj} - \left(\frac{\partial F}{\partial x}\right)^{n+1/2}_{i,jj-1}\right\}$. Since the magnitudes of the eigenvalues of $L_y(\Delta t_x/M)$ are bounded by unity, those of $L_{xy}(m, \Delta t_x/M)$ are at worst bounded by $1 + O(\Delta t_x)$ (von Neuman condition Eq. (5)).

NUMERICAL RESULTS

To illustrate the concepts of the previous sections numerical solutions of the two-dimensional interaction of an oblique shock wave with a laminar boundary layer at a Mach number of 2.0 will be presented and compared with the experimental data of Hakkinen. Some characteristic features of this interaction are illustrated schematically in Fig. 3. Hakkinen's data were chosen because the boundary layer is laminar throughout the interaction region and the experimental data include both plate surface pressure and skin friction. Two test cases, one in which the incident shock was not strong enough to cause flow separation, and one with a shock sufficiently strong to cause separation (Fig. 3), were solved numerically.

The computational rectangular mesh covered an area of 8.636 cm x 1.270 cm including 7.874 cm of plate. The boundary conditions were: (a) the upstream boundary values were initially set for uniform flow and thereafter held fixed; (b) the values of the boundary opposite the plate were initially set using inviscid oblique shock wave theory such that a shock of given strength and point of incidence on the plate would be generated and thereafter were held fixed; (c) the downstream exit boundary values were set equal to those just upstream after each step; and (d) for the boundary containing the plate a fictitious row of cells together with "mirror symmetry" was employed; that is, the plate was located midway between the row of fictitious points, denoted by j = 1, and the first interior row of points,

$j = 2$ (located $\Delta y/2$ off the plate). The $\rho_{i,1} = \rho_{i,2}$, $u_{i,1} = -u_{i,2}$, $v_{i,1} = -v_{i,2}$, $T_{i,1} = T_{i,2}$ and $p_{i,1} = p_{i,2}$ except for those points upstream of the plate where $u_{i,1} = u_{i,2}$. Boundary condition (c) assumes uniform flow at the exit. This is good near the plate. Away from the plate the flow field is supersonic and errors made at the boundary will not propagate upstream. By the temperature and density boundary conditions (d) the plate is treated as an adiabatic wall. The initial condition of the interior points is uniform flow. The Sutherland viscosity law for air, with $\lambda = -\frac{2}{3}\mu$, the perfect gas equation of state, and a constant Prandtl number equal to 0.72 were used.

Unseparated Flow

For this case, the pressure ratio, p_f/p_o (final (after reflection) to initial), was 1.2, the distance from the leading edge to the incident shock, x_s, was 4.88 cm, and the free-stream Reynolds number, Re_{x_s}, was 2.84×10^5. From Eqs. (8) and (9) with v taken as $v_1/2$ and u/v as u_1/v_1, where u_1 and v_1 are the velocity components after the incident shock and away from the plate, the estimates $\Delta x = 0.0848$ cm and $\Delta y = 0.0024$ cm for the boundary layer region are obtained as a reference.

An initial calculation with a mesh of 34 x 12 cells, $\Delta x = 0.254$ cm, $\Delta y = 0.127$ cm (more than 50 times larger than the estimate), was made using Eqs. (6) with $\Delta t = 0.9$, the maximum allowed by Eq. (3) ($u = u_1$, $v = v_1$ and $c = c_1$) and allowed to run 128 time steps when there was little change occurring in the flow field (approximately 5 minutes in machine time on the IBM 360/67). Figure 4 compares the numerical results with Hakkinen's data, where the surface pressure is approximated by $p_{i,1}$ and the local coefficient of skin friction by $\{\mu_{i,1}(u_{i,2} - u_{i,1})/\Delta y\}/(\rho_o u_o^2/2)$. The results for skin friction are in conspicuously poor agreement with experiment. Although the full set of Navier-Stokes equations was differenced, the coarseness of the mesh allowed the viscous terms to be swamped by truncation and round-off error. The numerical solution was essentially that of inviscid flow and the shock wave angles, strengths, etc., were within a few percent of inviscid theory. The calculation was then repeated; this time with a mesh of 34 x 32 cells containing a fine mesh near the plate, large enough to contain the estimated boundary layer and a coarse mesh away from the plate (Fig. 5). In the fine mesh of 34 x 22 cells $\Delta x = 0.254$ and $\Delta y = 0.00635$ cm, (approximately three times that estimated by Eqs. (8) and (9), and in the coarse mesh $\Delta x = 0.254$ and $\Delta y = 0.127$ cm. The solution was advanced in time separately for each mesh. First the fine mesh was advanced in time by $\Delta t_x = 0.9\ \Delta x/(|u_o| + c_o)$ using Eqs. (11) with $M = 20$. The row of cells, $j = 22$, was used as a boundary for the fine mesh. Data for these points were obtained by linear interpolation between points of the inner fine mesh and outer coarse mesh after each $\Delta t_x/M$ time step. After the inner mesh has been advanced in time by Δt_x, Eqs. (10) with $\Delta t = \Delta t_x$ are used in second order fashion to advance the outer mesh. During the calculation of the inner mesh transport through and stress at the boundary common to both meshes were saved. Their net transport and stress were then used as a boundary condition for the outer flow field. Thus, mass, momentum, and energy were rigorously conserved within the overall mesh. The basic assumption in using this mesh is that the viscous terms are important only in the boundary layer (although their effects are important away from the plate as well), thus allowing the outer flow field to be treated as inviscid by use of a coarse mesh. The numerical results for this calculation are displayed in Fig. 6. Figure 6(a) illustrates the asymptotic convergence in time from the initial condition to steady state of a velocity profile at $x = 4.699$ cm (the column of mesh points just upstream of the shock). Figure 6(b) compares the numerical results after 256 Δt_x time steps (four hours of machine time) with the experimental measurements of surface pressure and skin friction. Figure 6(c) shows the streamlines in the boundary layer obtained from the velocity fields using a third order interpolation subroutine and plotted on a cathode ray display tube. They are initially 0.00953 cm apart. Also contained in the figure are u—velocity profiles at $x = 2.794$, 5.080, 6.985 cm.

Separated Flow

The experimental conditions for this case were essentially the same as those for the separated case, $x_s = 4.953$ cm, $Re_{x_s} = 2.96 \times 10^5$, except the incident shock was stronger. $p_f/p_o = 1.40$. As before, using Eqs. (8) and (9) the estimates $\Delta x = 0.0238$ and $\Delta y = 0.00127$ cm

can be obtained as reference values.

Again, exactly as in the unseparated case the solution was advanced in time on a mesh containing a fine sub mesh where $\Delta x = 0.254$ and $\Delta y = 0.00635$ (approximately ten and five times that estimated) and a coarse sub mesh where $\Delta x = 0.254$ and $\Delta y = 0.127$ cm and allowed to run until there was little change occurring in the flow field (320 Δt_x time steps). The results are contained in Fig. 7. Although the computed separation point agrees well with the experimental point, the length of the separated region is underpredicted and the characteristic plateau in the experimental pressure profile is not found in the numerical data. Two related probable causes for this are: (a) there were too few points in the separated region (four cells) to provide good spatial resolution, and (b) Δx is more than ten times that estimated from Eq. (9). The mesh was further refined by halving Δx. The new mesh of 38 x 32 cells began 2.54 cm downstream of the leading edge and covered an area of 4.826 x 1.270 cm^2. The new time increment Δt_x was half that of the former and M equalled ten. The upstream boundary condition was obtained from the previous calculation and thereafter held fixed. The initial condition was the previous converged solution with second order interpolation used to define values at the additional points. It was observed that the solution on the new mesh, initially out of equilibrium, converged asymptotically again in about 256 additional time steps. The new results are shown in Fig. 8. The streamlines of Fig. 8(c) are initially 0.00953 cm apart and the u—velocity profiles are located at x = 2.794, 5.080, 5.715, and 6.985 cm.

CONCLUDING REMARKS

1. Although the conditions of consistency and stability are sufficient for convergence of the numerical solution to the exact solution for well-posed linear problems as mesh and time increments tend to zero, there is no guarantee that this will occur in nonlinear problems. The numerical analyst must at present be content with assuming the same behavior for the nonlinear case. The test cases in the applications section support this. It is felt that mesh spacings nearer those estimated by Eqs. (3) and (9) would cause the remaining disparity between the numerical and experimental results (i.e., the plateau in the pressure profile of Fig. 8) to be reduced. Nevertheless, good agreement in general has been achieved.

2. The techniques developed from the concept of splitting are expected to have much more general application than just those with severe differences in coordinate mesh spacing. Not only do they exhibit more flexibility to allow better matching of dependence domains, but since $\min(\Delta x/(|u| + c), \Delta y/(|v| + c)) \geq (|u|/\Delta x + |v|/\Delta y + c\sqrt{1/\Delta x^2 + 1/\Delta y^2})^{-1}$ their time step increments can be larger than the unsplit techniques. There are however two questions to their unrestricted use: (a) Although there is no loss in order of accuracy, are they still less accurate for practical choice of Δx and Δy; and (b) although the solution can proceed at larger time steps, is the computation time per step correspondingly greater also? To partially answer these questions the calculation which produced the data contained in Fig. 5 obtained by the unsplit Eqs. (6) was recalculated using the split Eqs. (10) for the same simple 34 x 12 mesh. The steady-state solutions were nearly identical (Fig. 9). The time step ratio, $\Delta t_x/\Delta t$, equalled 1.45 where Δt_x was taken as $0.9\Delta x/(|u_o| + c_o)$ and the computation time per step ratio, $t_{unsplit}/t_{split}$, was 0.924. Thus for the case computed here the computation time to advance the solution to a given time by the split technique is 0.75 that of the unsplit technique.

REFERENCES

Hakkinen, R. J.; Greber, I.; Trilling, L.; and Abarbanel, S. S.: The Interaction of an Oblique Shock Wave with a Laminar Boundary Layer. NASA Memo 2-18-59W, 1959.

Kutler, P.: Application of Selected Finite Difference Techniques to the Solution of Conical Flow Problems. Ph.D. thesis, Iowa State Univ., 1969.

MacCormack, R. W.: The Effect of Viscosity in Hypervelocity Impact Cratering. AIAA Paper No. 69-354, 1969.

Peaceman, D. W.; and Rachford, H. H., Jr.: The Numerical Solution of Parabolic and Elliptic Differential Equations. SIAM Jour., vol. 3, 1955, pp. 28-41.

Yanenko, N. N.: The Method of Fractional Steps for Numerical Solution of the Problems of Mechanics of Continuous Media. Fluid Dynamics Transactions, vol. 4, 1969, pp. 135-147. Institute of Fundamental Technical Research, Polish Academy of Science, Warsaw.

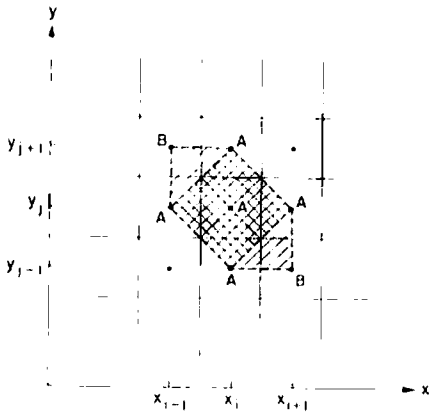

Fig. 1. Star of mesh points involved in a single application of Eqs. (2).

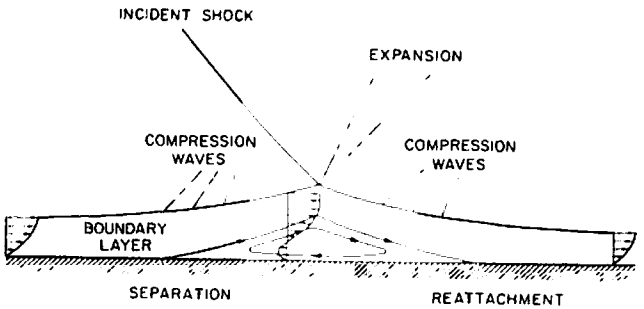

Fig. 3. Sketch of shock boundary layer interaction.

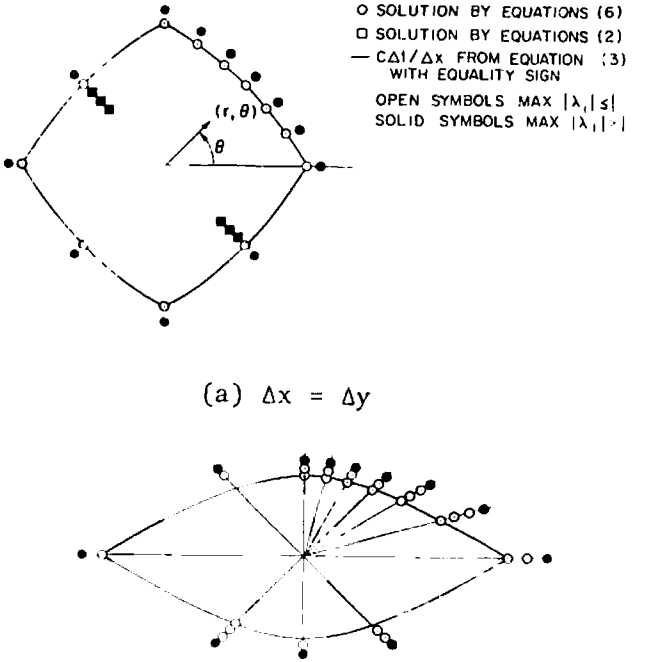

(a) $\Delta x = \Delta y$

(b) $\Delta x = 10\ \Delta y$

Fig. 2. Stability domain, $c\ \Delta t/\Delta x$ vs. $\theta = \arctan(v/u)$ at Mach 2.0.

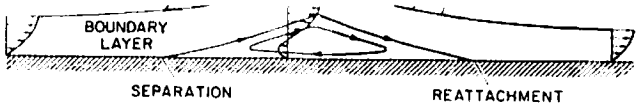

Fig. 3. Sketch of shock boundary layer interaction.

Fig. 2. Stability domain, c $\Delta t/\Delta x$ vs. θ = arctan(v/u) at Mach 2.0.

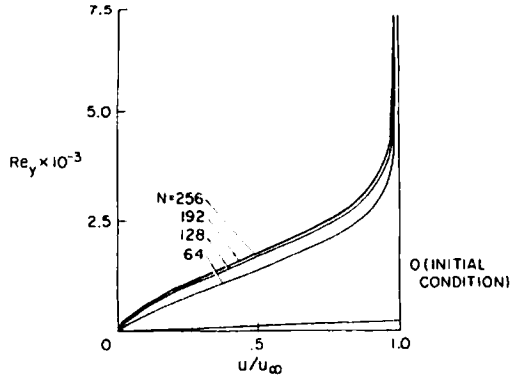

(a) Development of velocity profiles at $Re_x = 2.74 \times 10^5$ with time.

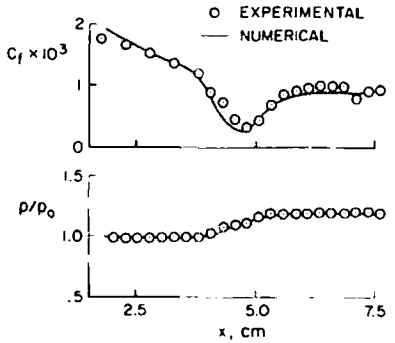

(b) Skin-friction coefficient and surface pressure.

Fig. 6. Numerical results with fine inner mesh coupled to coarse outer mesh; $p_f/p_o = 1.2$.

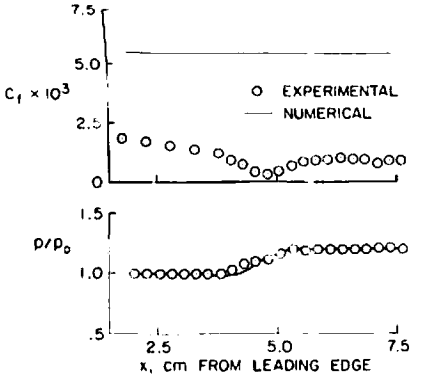

Fig. 4. Comparison of numerical and experimental results; $p_f/p_o = 1.2$, $\Delta x = 0.254$ and $\Delta y = 0.127$ cm.

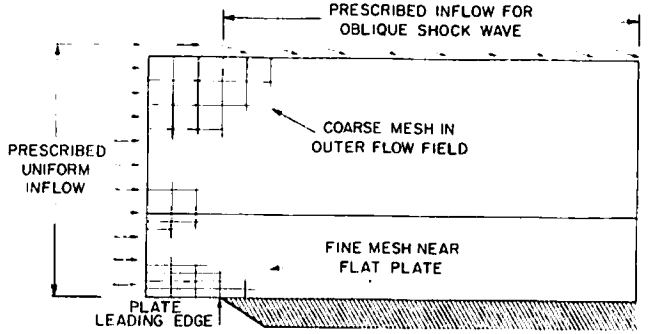

Fig. 5. Mesh setup.

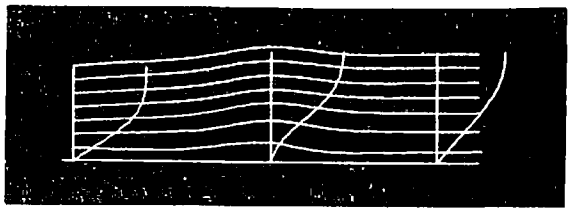

(c) Streamlines and velocity profiles.

Fig. 6. Concluded.

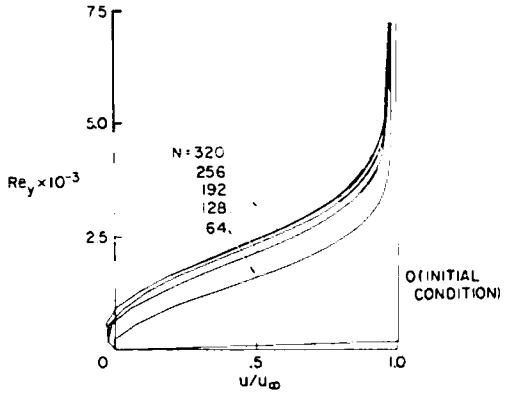

(a) Development of velocity profiles at $Re_x = 2.79 \times 10^5$ with time.

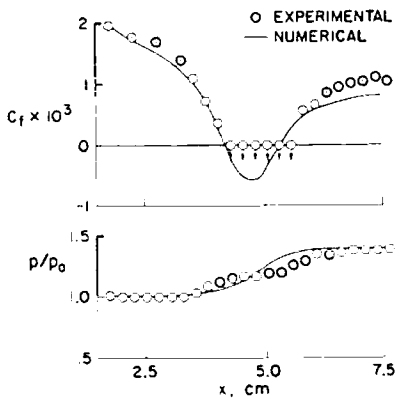

(b) Skin-friction coefficient and surface pressure.

Fig. 7. Numerical results for $p_f/p_o = 1.4$; $\Delta x = 0.254$ and $\Delta y = 0.00635$ cm in fine mesh, $\Delta x = 0.254$ and $\Delta y = 0.127$ cm in coarse mesh.

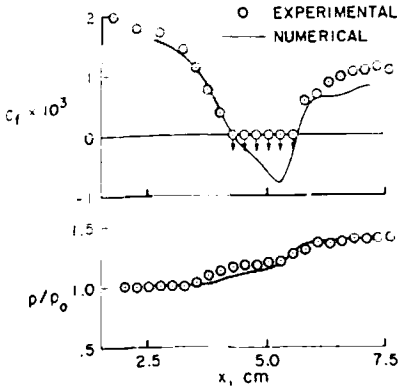

(a) Skin-friction coefficient and surface pressure.

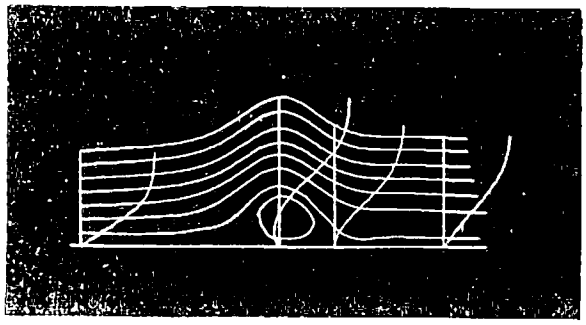

(b) Streamlines and velocity profiles.

Fig. 8. Numerical results for $p_f/p_o = 1.4$; $\Delta x = 0.127$ and $\Delta y = 0.00635$ cm in fine mesh, $\Delta x = 0.127$ and $\Delta y = 0.127$ cm in coarse mesh.

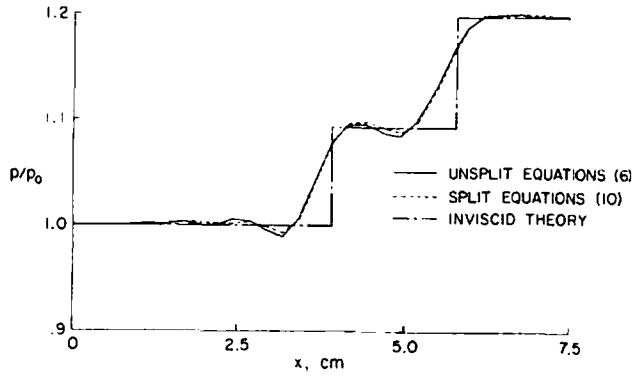

Fig. 9. Comparison of pressure profiles at $y = 0.5715$ cm from plate.